Hybrid plasmonic structures based on CdS nanotubes: a novel route to low-threshold lasing on the nanoscale

2012 J. Phys. D: Appl. Phys. 45 505105

(http://iopscience.iop.org/0022-3727/45/50/505105)

IOP Publishing | Journal of Physics D: Applied Physics

J. Phys. D: Appl. Phys. **45** (2012) 505105 (7pp) doi:10.1088/0022-3727/45/50/505105

Hybrid plasmonic structures based on CdS nanotubes: a novel route to low-threshold lasing on the nanoscale

Yusheng Bian[1], Zheng Zheng[1], Xin Zhao[1], Yalin Su[1], Lei Liu[1], Jiansheng Liu[1], Tao Zhou[2] and Jinsong Zhu[3]

[1] School of Electronic and Information Engineering, Beihang University, Beijing 100191, People's Republic of China

[2] Department of Physics, New Jersey Institute of Technology, Newark, NJ 07102, USA

[3] National Center for Nanoscience and Technology, No 11 Zhongguancun Beiyitiao, Beijing 100190, People's Republic of China

E-mail: zhengzheng@buaa.edu.cn

Received 4 August 2012, in final form 12 October 2012
Published 19 November 2012
Online at stacks.iop.org/JPhysD/45/505105

Abstract

Nanowires and nanotubes could become important building blocks in advanced photonic systems owing to their fascinating optoelectronic properties and high compatibility with versatile chemical synthetic methods. Many intriguing studies have been enabled by applying these nanostructures in the construction of various types of active and passive photonic components. Successful examples are the recent demonstration of semiconductor and plasmonic lasers based on CdS nanowires (Duan *et al* 2003 *Nature* **421** 241–5, Oulton *et al* 2009 *Nature* **461** 629–32, Ma *et al* 2010 *Nature Mater.* **10** 110–13), which generate and deliver intense coherent light down to and even below the diffraction-limited scale. Here in this paper, by carrying out a numerical investigation of a novel hybrid plasmonic structure that consists of a CdS nanotube sitting above a metal substrate separated by a nanometric MgF_2 layer, we show theoretically that nanotube-based plasmonic structures can also act as highly efficient lasing sources. Optical properties of such a laser configuration including modal behaviour and the lasing threshold is investigated with regard to the variation of key geometrical parameters. Simulation results reveal that the employment of a CdS nanotube may result in improved optical performance compared with the conventional CdS-nanowire-based plasmon laser. Reduced lasing threshold with mitigated modal loss can be achieved simultaneously under carefully engineered geometries. We also explore the feasibility of combining nanowire- and nanotube-based active and passive components for on-chip integrations. As a simple demonstration, monolithic integration of a CdS nanotube laser with a CdS-nanowire-based passive component is shown numerically on a single chip. We expect that these studies could lay the foundations for nanotube- and nanowire-based hybrid integrated photonic components and circuits.

(Some figures may appear in colour only in the online journal)

1. Introduction

Recent advancement in laser science has been continuously producing new types of coherent light sources with unprecedented fascinating features. Future nanolasers require configurations capable of achieving higher power, faster response, miniaturized physical dimensions and/or reduced output mode size [1, 4–14]. Semiconductor nanowire based structures are among those most promising microscopic lasers with ~wavelength scale yielded optical modes [1, 5, 14]. Among a diverse range of semiconductors, II–VI (e.g. CdS and ZnO) and III–V materials (e.g. GaN) are the most preferable choices for nanowire lasing, due to their significantly strong exciton binding energy to ensure efficient laser actions. Along with their availability with versatile existing chemical methods [15], these structures get widely used in many areas of physical science and engineering. However, like other dielectric-based structures such as photonic crystal cavity lasers [6], they are fundamentally subjected to the diffraction limit, which restricts further downscaling of either their physical scale or generated optical mode size below the wavelength level.

A promising solution to overcome the above challenge is by exploiting the surface plasmon (SP) effect, which offers unique capabilities for guiding and controlling light down to the sub-diffraction-limited scale [16–19]. Further miniaturization of microscopic lasers could also be realized with versatile structures involving SPs. Examples of recent achievements are the plasmon lasers based on localized SP [20] and propagating SP effect [2, 3], whose physical size and mode width directly reach the nanometre scale well beyond the diffraction limit. For these propagating SP-based plasmon lasers, their features are dominated by the optical properties of the plasmonic waveguiding configurations involved. These hybrid plasmon polariton (HPP) structures, typically consisting of high-index dielectrics placed in close proximity to metallic surfaces, are able to achieve subwavelength confinement and long-range propagation distance simultaneously [21–24]. Highly efficient laser action could be enabled by replacing the dielectric with a gain medium, together with the introduction of a proper feedback mechanism, such as Fabry–Perot or whispering gallery cavities [2, 3].

In addition to leveraged as efficient lasing sources, hybrid structures also exhibit useful applications in light guiding, mode splitting as well as other areas. Various hybrid guiding schemes [21–39] and a number of integrated photonic components [40–45] have been presented and studied intensively. While most HPP structures claim to be compatible with standard fabrication methods, many are rather challenging to realize, despite the fact that they might exhibit improved optical performance over the conventional hybrid waveguide in a certain aspect. Such a drawback hinders the migration of these devices from theoretical predictions to practical implementations.

Here in this paper, we propose and investigate a novel hybrid plasmonic structure comprised of a CdS nanotube atop a MgF_2-coated silver surface. Such a hybrid waveguide shares a similar fabrication procedure as that of the typical CdS-nanowire-based plasmonic structure, which can be readily implemented by placing a CdS nanotube onto a MgF_2-coated silver substrate. The CdS nanotube can be fabricated using various strategies, including surfactant-assisted synthesis [46], chemical bath deposition [47], arc-electrodeposition technique [48], microwave and ultrasonic irradiation [49, 50], electrodeposition and dissolution route [51], as well as the chemical vapour deposition (CVD) template method [52]. Through numerical analysis, we show theoretically that these CdS-nanotube-based plasmonic structures are also capable of supporting low-loss transportation of hybrid modes on the subwavelength scale. With the optimization of the geometry size and taking into consideration the cross-sectional shape, a highly efficient lasing source exhibiting even better optical behaviour could be achieved compared with the CdS-nanowire-based laser structure.

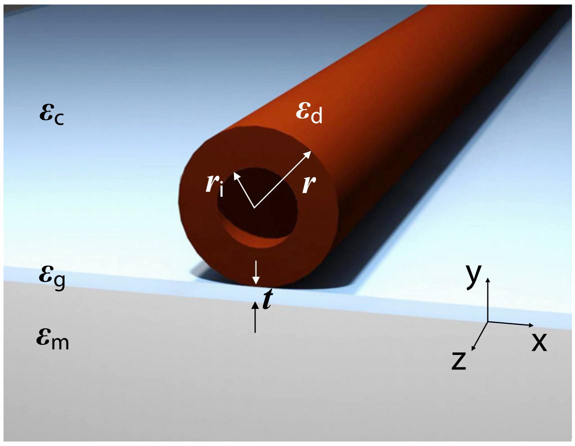

Figure 1. Hybrid plasmon laser structure based on a circular CdS nanotube.

2. Optical properties of the proposed nanotube-based hybrid plasmon laser structure

Figure 1 shows the geometry of the studied hybrid plasmon laser, where a circular-shaped CdS nanotube sits above a low-index nanometre-thick, dielectric-coated, metallic substrate. The inner and outer radii of the nanotube are r_i and r, respectively, while the radius ratio of r_i to r is defined as a. The thickness of the low-index dielectric coating layer is t. Optical characteristics of the hybrid mode supported by the structure are studied at a wavelength of $\lambda = 489$ nm in this paper, which corresponds to the CdS I_2 exciton line [2, 53]. The metallic substrate is assumed to be silver (Ag), the low-index dielectric gap layer is MgF_2 and the cladding is made of air. The permittivities of air, MgF_2, CdS and Ag are $\varepsilon_c = 1$, $\varepsilon_d = 1.96$, $\varepsilon_g = 5.76$ and $\varepsilon_m = -9.3 + 0.2i$ [54], respectively. The modal properties are investigated by carrying out a 2D modal analysis for the cross-section of the laser configuration based on the finite-element method (FEM) using COMSOL^{TM}. The eigenmode solver is applied with the scattering boundary condition. Convergence tests are performed to ensure that the numerical boundaries and meshing do not interfere with the solutions. Based on the 2D modal analysis, the pumping threshold of the laser could also be obtained.

Electric field distributions of the fundamental quasi-TM plasmonic mode is shown schematically in figure 2. Pronounced field enhancement is seen clearly in the MgF_2 gap owning to the strong hybridization between dielectric and SP modes. While the index contrast inside the nanotube also results in a locally enhanced electric field in the air-filled hollow area, although much weaker than that observed in the gap. These electric field plots indicate strong overall confinement achievable in the gap region with sufficient modal overlap in the semiconductor to facilitate gain. The existence of the hollow area in the nanotube also exhibits the effect of releasing the mode field into the low-index air region, hence showing the potential to further reduce the propagation loss.

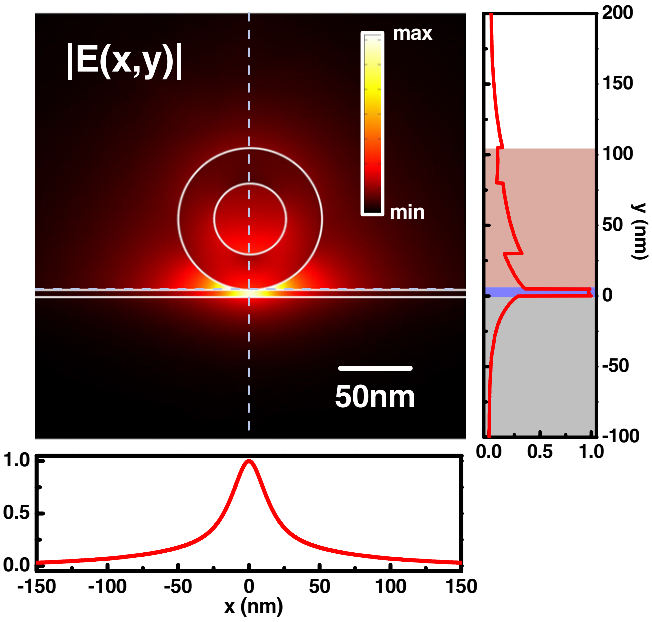

Figure 2. Simulated electric field ($|E(x, y)|$) distribution of the fundamental hybrid plasmonic mode of the studied structure at a wavelength of 489 nm, where $r = 50$ nm, $a = 0.5$, $t = 5$ nm. The cross-sectional fields along the dashed lines in the field map are plotted to better illustrate the mode confinement inside the gap and the CdS nanotube.

The modal properties including the modal effective index (n_{eff}), effective propagation loss (α_{eff}), normalized mode area (A_{eff}/A_0) and confinement factor (Γ) of the hybrid plasmonic mode supported by the nanotube-based structure are shown in figures 3(*a*) and (*b*) as the size of the nanotube varies. The outer radius of the nanotube is set within the range 40–60 nm in order to ensure simultaneous realization of low pumping threshold and single mode operation. The modal effective index and the effective propagation loss are determined from the real and imaginary parts of the eigenvalue. The confinement factor and the mode area can be derived by means of post-processing based on the calculated mode profiles. Here, the confinement factor (Γ) is defined as the ratio of the electric energy in the CdS material of the nanotube and the total electric energy of the mode. The effective mode area is calculated using $A_{eff} = (\iint |E|^2\, dx\, dy)^2/(\iint |E|^4\, dx\, dy)$. A_0 is the diffraction-limited mode area in free space and defined as $\lambda^2/4$. It is shown that for structures with different r, the modal effective index, confinement factor and mode area exhibit monotonical trends when the hollow area of the nanotube increases. Reduced n_{eff} and Γ, together with increased A_{eff}, are signatures of gradually weakened mode confinement with the increase in r_i. The propagation loss, however, demonstrates quite different trends for different r. Geometry with a small nanotube ($r = 40$ and 50 nm) shows a reduced propagation loss at larger r_i. While on the other hand, when $r = 60$ nm, a local maximum is observed in the curve of the propagation loss at a critical ratio a. This is an indication of the occurrence of strongest coupling between the nanotube mode and the plasmonic mode, where the effective indices of the two modes match each other, as also seen in many other hybrid plasmonic structures [21, 36, 37]. The reason why no such coupling condition happens for the small nanotube case is the relatively small effective index of the nanotube mode, which gets even smaller when the hollow region increases, thus leading to a further mismatch between the dielectric and plasmonic modes and consequently the monotonical change in the coupling strength. For $r = 60$ nm, further increasing the size of the hollow region over that critical value leads to a continuous reduction in α_{eff}, similar to that observed in the smaller nanotube case. It is also illustrated in figure 3(*a*) that within a wide range of radius ratios, the confinement factor maintains a relatively high value all the time. For the case of $r = 60$ nm, Γ is still as large as 0.3 even when a gets close to 0.7, indicating that a substantial amount of electric energy resided in the CdS material. Such a strong modal overlap between the hybrid mode and the gain medium, together with the reduced propagation loss, offers great promise for low pumping threshold.

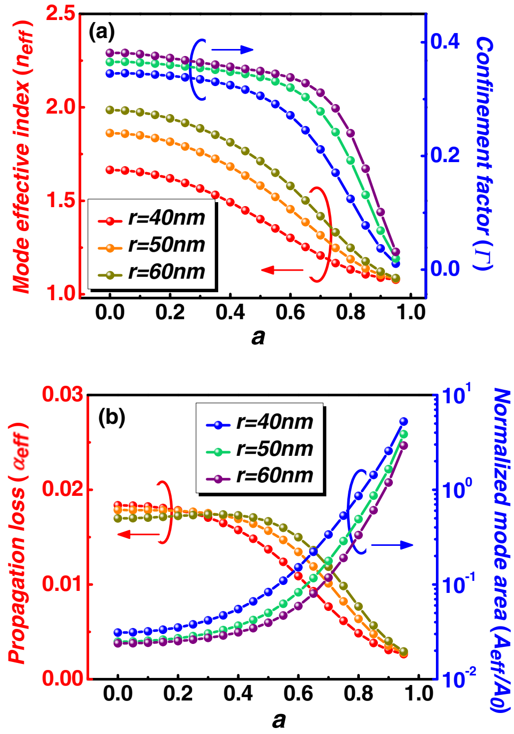

Figure 3. Dependence of the modal properties of the fundamental hybrid plasmonic mode on the size of the CdS nanotube: (*a*) modal effective index (n_{eff}) and confinement factor (Γ); (*b*) propagation loss (α_{eff}) and normalized mode area (A_{eff}/A_0). The extreme case of $a = 0$ corresponds to the CdS-nanowire-based hybrid plasmonic structure.

Based on the above discussions of modal properties, we further investigate the lasing threshold of the hybrid structure. Here, the amplitude threshold gain is calculated using $g_{th} = (k_0\alpha_{eff} + \ln(1/R)/L)/\Gamma \cdot (n_{eff}/n_{tube})$ [23], where $k_0 = 2\pi/\lambda$ and n_{tube} is the refractive index of the nanotube. The nanotube length L is assumed to be 30 μm, while the end facet reflectivity is estimated using $R = (n_{eff} - 1)/(n_{eff} + 1)$. These approximations are adopted to simply illustrate the effect of geometric parameters on lasing properties rather than predict the accurate pump threshold. Calculated results in figure 4 indicate that, as long as the radius ratio a is not very large, the lasing threshold decreases monotonically with the increase

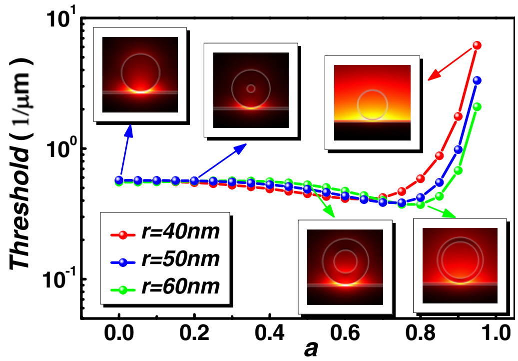

Figure 4. Lasing threshold (g_{th}) of the hybrid mode for the CdS-nanotube-based structure under varied configuration parameters, where the extreme case of $a = 0$ corresponds to the CdS-nanowire-based plasmonic structure. The insets plot the corresponding electric field distributions of the output optical mode; upper insets, from left to right: $r = 50$ nm, $a = 0$; $r = 50$ nm, $a = 0.2$; $r = 40$ nm, $a = 0.95$; lower insets, from left to right: $r = 60$ nm, $a = 0.5$; $r = 60$ nm, $a = 0.8$.

in the hollow area for the cases of small nanotubes ($r = 40$ and 50 nm), which is largely due to the maintained overall confinement in the gain material and the significantly reduced propagation loss. While for a larger nanotube ($r = 60$ nm), a slightly increased pumping threshold is observed when a is small, which is caused by the increase in the propagation loss exhibited below the critical radius ratio shown in figure 3(*b*). As a gets larger, the mitigated modal loss and the strong confinement would bring the threshold gain back to a low level. For all the studied cases, the minimum pumping threshold is observed at a relatively large a, where over 30% threshold reduction could be achieved compared with the nanowire plasmon laser. Beyond such a critical radius ratio, the g_{th} curve would rise sharply. The dramatically increased gain needed for lasing is caused by the highly weakened mode confinement when the hollow region is very large (as also shown in the electric field distribution in the inset), which has become the dominant factor that determines the lasing properties. As also indicated from figures 3(*b*) and 4, low-threshold laser actions could be enabled on a subwavelength scale as long as a is not very large.

Depending on the specific fabrication method, CdS nanotubes may also have other cross-sectional shapes in addition to the circular one as assumed in the above studies. The most commonly obtained types during synthesis are the hexagonal-shaped CdS nanotube [46, 50, 52]. Although CdS 1D nanostructures with square-like cross-sections have only been demonstrated in solid styles, such as nanobelts [3, 55] and nanoribbons [56, 57], yet it is still interesting to see the optical performance of a square-shaped nanotube-based plasmon laser. Here the modal properties and lasing thresholds of hybrid plasmon lasers leveraging hexagonal or square CdS nanotubes are also investigated using a similar method to that employed for the circular case. Both the side length of the hexagonal nanotube and the half-width for the square structure are denoted as w (both fixed at 50 nm), while other parameters are defined in the same way as in the circular case. The calculated modal properties shown in figures 5(*a*) and (*b*)

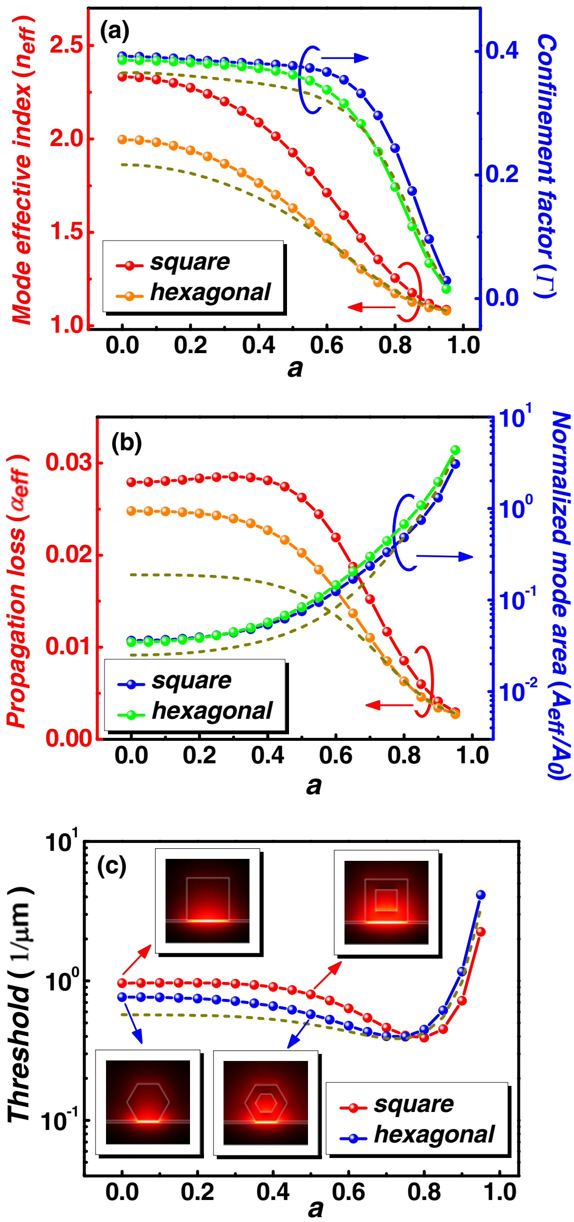

Figure 5. Optical properties of the fundamental hybrid plasmonic mode for the square-shaped and hexagonal-shaped CdS nanotube structures under varied configuration parameters (where the extreme case of $a = 0$ corresponds to the CdS-nanowire-based plasmonic structure): (*a*) modal effective index (n_{eff}) and confinement factor (Γ); (*b*) propagation loss (α_{eff}) and normalized mode area (A_{eff}/A_0); (*c*) lasing threshold (g_{th}) of the hybrid mode The dark-yellow dashed lines correspond to the modal property and threshold of a circular-shaped CdS nanotube laser with $r = 50$ nm (as shown in figure 4). The insets plot the corresponding electric field distributions of the output optical mode; upper insets, from left to right: $2w = 100$ nm, $a = 0$; $2w = 100$ nm, $a = 0.5$; lower insets, from left to right: $w = 50$ nm, $a = 0$; $w = 50$ nm, $a = 0.5$.

indicate that similar modal behaviour could be achieved for the hexagonal or square structure compared with the circular nanotube case (illustrated in dark-yellow dashed lines). The only difference is the non-monotonical trend observed in the propagation loss of the square nanotube, which is caused by the change in the coupling strength during the variation of a, similar to the circular CdS structure with $r = 60$ nm.

Correspondingly, the lasing threshold of the square case increases first before it decreases when the structure evolves from the nanowire type ($a = 0$) to the nanotube type with an increased hollow region, as seen in figure 5(*c*). While for both the square and hexagonal nanotubes, the lowest pumping threshold occurs when the radius ratio is relatively large. Furthermore, in contrast to the circular nanotube plasmon laser, structures employing hexagonal or square-shaped nanotubes achieve more significant reduction in the lasing threshold when compared with the nanowire-based configuration, i.e. as large as 50% for the hexagonal nanotube plasmon laser, and even up to 60% for the square nanotube case.

It is worth mentioning that, in addition to tailoring the lasing properties through control of geometric parameters and shape, new features may also be added to the plasmon laser by incorporating other materials into the hollow region of the CdS nanotube. For instance, carbon nanotubes/CdS coaxial nanowires [58] and ZnO/CdS core/shell nanowire heterostructures [59] are among these interesting structures that could probably bring new functionalities to laser actions.

CdS nanowires have been widely employed as promising candidates to build highly efficient optoelectronic components with a wide range of useful applications [60, 61]. Here, we show the possibility of integrating such a CdS nanotube laser structure with passive CdS nanowire components. Three-dimensional (3D) FEM simulations are performed to mimic the operation of the hybrid photonic system for on-chip integrations. In order to perform a full 3D numerical simulation of the mode propagation along the CdS nanotube and coupling of the nanotube mode into nanowire-based configurations, the field distribution from the 2D eigenmode solver of a nanotube-based plasmonic waveguide is set as a source boundary condition for the 3D analysis. Other boundaries of the computational region are applied with perfect electric conductor boundary conditions with $n \times E = 0$. Fine meshes with a maximum mesh size around $\lambda/50$ are adopted in the nanotube, nanowire and the gap regions, while relatively coarser meshes are used for other sub-domains. Here it is worth mentioning that our main focus of such a simulation is to reveal the feasibility of mode transmission and evolution in a simple nanophotonic chip based on nanotubes and nanowires, assuming that the laser beam is efficiently coupled into the nanotube as the input optical mode. The processes of pumping the laser device and generation of the laser beam are not included in our current simulations. While for practical experiments, a similar excitation method to that reported in [2] could be adopted. By using a mode-locked Ti–sapphire laser along with an objective lens, the pump beam can be focused and illuminated directly on the sample to excite laser oscillation. As seen in figure 6, the plasmonic mode could propagate along the hybrid CdS nanotube plasmonic structure with low loss and also couple efficiently (more than 80% of the total power) to a near-by (several hundred nanometres away) Y-branched structure consisting of two CdS nanowires on top of a MgF_2–Ag substrate. More complex photonic nanocircuits may be realized by integrating the CdS nanotube light source with various other passive components such as a ring-resonator, Bragg grating to achieve versatile functionalities. Furthermore, the merging of metallic nanowires with CdS 1D nanostructures represents another pathway that may bring new capabilities to CdS-based hybrid integrated nanoscale photonic systems [40, 62–64].

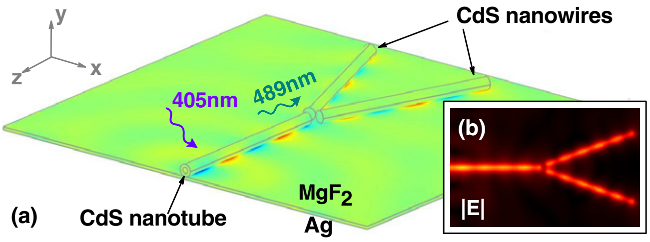

Figure 6. Example of circular-shaped CdS nanotube and nanowire based hybrid optical nanocircuits with the functionality of lasing and power splitting by monolithic integration of the CdS nanotube nanolaser and Y-shaped CdS nanowires on a single Ag–MgF_2 chip. (*a*) *Z* component of the electric field distribution of the 3D structure. The wavy arrows schematically illustrate the pumping of the CdS nanotube laser configuration at 405 nm wavelength and laser emission at 489 nm in the experimental setup, while such processes are not included in the current simulations; (*b*) 2D normalized electric field plot along the metallic surface (*X*–*Z* plane).

3. Conclusions

In conclusion, we have investigated the feasibility of building highly efficient hybrid plasmon lasers based on CdS nanotubes. Numerical studies show that compared with the conventional nanowire-based laser structure, the hybrid configuration leveraging CdS nanotube could enable nanoscale lasing with even lower pumping threshold at the optical frequency, meanwhile maintaining the subwavelength generated optical mode size together with dramatically mitigated modal loss. To reveal its usage in hybrid integrated photonic systems, we also explore the possibility of integrating such a nanotube laser structure with passive CdS components. We expect that these investigations could be useful for the development of nanotube- and nanowire-based integrated photonic circuits.

Acknowledgments

This work was supported by the 973 Program (2009CB930701), the NSFC (60921001/61077064), the National Key Scientific Instruments and Equipment Development Special Fund Management (2011YQ0301240502) and Scholarship Award for Excellent Doctoral Student granted by the Ministry of Education at Beihang University.

References

[1] Duan X F, Huang Y, Agarwal R and Lieber C M 2003 Single-nanowire electrically driven lasers *Nature* **421** 241–5
[2] Oulton R F, Sorger V J, Zentgraf T, Ma R M, Gladden C, Dai L, Bartal G and Zhang X 2009 Plasmon lasers at deep subwavelength scale *Nature* **461** 629–32
[3] Ma R-M, Oulton R F, Sorger V J, Bartal G and Zhang X 2010 Room-temperature sub-diffraction-limited plasmon laser by total internal reflection *Nature Mater.* **10** 110–13

[4] Drescher M, Hentschel M, Kienberger R, Tempea G, Spielmann C, Reider G A, Corkum P B and Krausz F 2001 X-ray pulses approaching the attosecond frontier *Science* **291** 1923–7
[5] Johnson J C, Choi H J, Knutsen K P, Schaller R D, Yang P D and Saykally R J 2002 Single gallium nitride nanowire lasers *Nature Mater.* **1** 106–10
[6] Altug H, Englund D and Vuckovic J 2006 Ultrafast photonic crystal nanocavity laser *Nature Phys.* **2** 484–8
[7] Hill M T *et al* 2007 Lasing in metallic-coated nanocavities *Nature Photon.* **1** 589–94
[8] Corkum P B and Krausz F 2007 Attosecond science *Nature Phys.* **3** 381–7
[9] Astafiev O, Inomata K, Niskanen A O, Yamamoto T, Pashkin Y A, Nakamura Y and Tsai J S 2007 Single artificial-atom lasing *Nature* **449** 588–90
[10] Zimmler M A, Bao J, Capasso F, Mueller S and Ronning C 2008 Laser action in nanowires: observation of the transition from amplified spontaneous emission to laser oscillation *Appl. Phys. Lett.* **93** 051101
[11] Hill M T *et al* 2009 Lasing in metal–insulator–metal sub-wavelength plasmonic waveguides *Opt. Express* **17** 11107–12
[12] Klein J and Kafka J D 2010 The Ti:sapphire laser: the flexible research tool *Nature Photon.* **4** 289
[13] Murphy E 2010 The semiconductor laser: enabling optical communication *Nature Photon.* **4** 287
[14] Vanmaekelbergh D and van Vugt L K 2011 ZnO nanowire lasers *Nanoscale* **3** 2783–800
[15] Yan R X, Gargas D and Yang P D 2009 Nanowire photonics *Nature Photon.* **3** 569–76
[16] Barnes W L, Dereux A and Ebbesen T W 2003 Surface plasmon subwavelength optics *Nature* **424** 824–30
[17] Ozbay E 2006 Plasmonics: merging photonics and electronics at nanoscale dimensions *Science* **311** 189–93
[18] Gramotnev D K and Bozhevolnyi S I 2010 Plasmonics beyond the diffraction limit *Nature Photon.* **4** 83–91
[19] Zhang J, Zhang L and Xu W 2012 Surface plasmon polaritons: physics and applications *J. Phys. D: Appl. Phys.* **45**
[20] Noginov M A, Zhu G, Belgrave A M, Bakker R, Shalaev V M, Narimanov E E, Stout S, Herz E, Suteewong T and Wiesner U 2009 Demonstration of a spaser-based nanolaser *Nature* **460** 1110–2
[21] Oulton R F, Sorger V J, Genov D A, Pile D F P and Zhang X 2008 A hybrid plasmonic waveguide for subwavelength confinement and long-range propagation *Nature Photon.* **2** 496–500
[22] Sorger V J, Ye Z, Oulton R F, Wang Y, Bartal G, Yin X and Zhang X 2011 Experimental demonstration of low-loss optical waveguiding at deep sub-wavelength scales *Nature Commun.* **2** 331
[23] Zhu L 2010 Modal properties of hybrid plasmonic waveguides for nanolaser applications *IEEE Photon. Technol. Lett.* **22** 535–7
[24] Bian Y S, Zheng Z, Liu Y, Zhu J S and Zhou T 2011 Coplanar plasmonic nanolasers based on edge-coupled hybrid plasmonic waveguides *IEEE Photon. Technol. Lett.* **23** 884–6
[25] Fujii M, Leuthold J and Freude W 2009 Dispersion relation and loss of subwavelength confined mode of metal-dielectric-gap optical waveguides *IEEE Photon. Technol. Lett.* **21** 362–4
[26] Dai D X and He S L 2009 A silicon-based hybrid plasmonic waveguide with a metal cap for a nano-scale light confinement *Opt. Express* **17** 16646–53
[27] Bian Y S, Zheng Z, Zhao X, Zhu J S and Zhou T 2009 Symmetric hybrid surface plasmon polariton waveguides for 3D photonic integration *Opt. Express* **17** 21320–5
[28] Avrutsky I, Soref R and Buchwald W 2010 Sub-wavelength plasmonic modes in a conductor-gap-dielectric system with a nanoscale gap *Opt. Express* **18** 348–63
[29] Alam M Z, Meier J, Aitchison J S and Mojahedi M 2010 Propagation characteristics of hybrid modes supported by metal-low-high index waveguides and bends *Opt. Express* **18** 12971–9
[30] Bian Y S, Zheng Z, Liu Y, Zhu J S and Zhou T 2010 Dielectric-loaded surface plasmon polariton waveguide with a holey ridge for propagation-loss reduction and subwavelength mode confinement *Opt. Express* **18** 23756–62
[31] Chen D 2010 Cylindrical hybrid plasmonic waveguide for subwavelength confinement of light *Appl. Opt.* **49** 6868–71
[32] Kwon M S 2011 Metal–insulator–silicon–insulator–metal waveguides compatible with standard CMOS technology *Opt. Express* **19** 8379–93
[33] Bian Y S, Zheng Z, Liu Y, Zhu J S and Zhou T 2011 Hybrid wedge plasmon polariton waveguide with good fabrication-error-tolerance for ultra-deep-subwavelength mode confinement *Opt. Express* **19** 22417–22
[34] Kim J T 2011 CMOS-compatible hybrid plasmonic waveguide for subwavelength light confinement and on-chip integration *IEEE Photon. Technol. Lett.* **23** 206–8
[35] Zou C-L, Sun F-W, Dong C-H, Xiao Y-F, Ren X-F, Lv L, Chen X-D, Cui J-M, Han Z-F and Guo G-C 2012 Movable fiber-integrated hybrid plasmonic waveguide on metal film *IEEE Photon. Technol. Lett.* **24** 434–6
[36] Bian Y S, Zheng Z, Zhao X, Su Y L, Liu L, Liu J S, Zhu J S and Zhou T 2012 Guiding of long-range hybrid plasmon polariton in a coupled nanowire array at deep-subwavelength scale *IEEE Photon. Technol. Lett.* **24** 1279–81
[37] Ta V D, Chen R and Sun H D 2011 Wide-range coupling between surface plasmon polariton and cylindrical dielectric waveguide mode *Opt. Express* **19** 13598–603
[38] Bian Y S, Zheng Z, Zhao X, Su Y L, Liu L, Liu J S, Zhu J S and Zhou T 2012 Highly confined hybrid plasmonic modes guided by nanowire-embedded-metal grooves for low-loss propagation at 1550nm *IEEE J. Sel. Top. Quantum Electron.* in press
[39] Rao R and Tang T 2012 Study of an active hybrid gap surface plasmon polariton waveguide with nanoscale confinement size and low compensation gain *J. Phys. D: Appl. Phys.* **45** 245101
[40] Guo X, Qiu M, Bao J, Wiley B J, Yang Q, Zhang X, Ma Y, Yu H and Tong L 2009 Direct coupling of plasmonic and photonic nanowires for hybrid nanophotonic components and circuits *Nano Lett.* **9** 4515–9
[41] Zhang X Y, Hu A, Wen J Z, Zhang T, Xue X J, Zhou Y and Duley W W 2010 Numerical analysis of deep sub-wavelength integrated plasmonic devices based on semiconductor–insulator–metal strip waveguides *Opt. Express* **18** 18945–59
[42] Chu H S, Li E P, Bai P and Hegde R 2010 Optical performance of single-mode hybrid dielectric-loaded plasmonic waveguide-based components *Appl. Phys. Lett.* **96** 221103
[43] Horvath C, Bachman D, Wu M, Perron D and Van V 2011 Polymer hybrid plasmonic waveguides and microring resonators *IEEE Photon. Technol. Lett.* **23** 1267–69
[44] Alam M Z, Aitchison J S and Mojahedi M 2012 Compact and silicon-on-insulator-compatible hybrid plasmonic TE-pass polarizer *Opt. Lett.* **37** 55–7
[45] Xiao Y-F, Li B-B, Jiang X, Hu X, Li Y and Gong Q 2010 High quality factor, small mode volume, ring-type plasmonic microresonator on a silver chip *J. Phys. B: At. Mol. Opt. Phys.* **43** 035402

[46] Rao C N R, Govindaraj A, Deepak F L, Gunari N A and Nath M 2001 Surfactant-assisted synthesis of semiconductor nanotubes and nanowires *Appl. Phys. Lett.* **78** 1853–5
[47] Zhang H, Ma X Y, Xu J and Yang D R 2004 Synthesis of CdS nanotubes by chemical bath deposition *J. Cryst. Growth* **263** 372–6
[48] Wang C, Fang J, He J and O'Connor C J 2003 Convenient arc-electrodeposition technique to synthesize CdS nanotubes at room temperature *J. Mater. Sci. Lett.* **22** 413–5
[49] Shao M W, Xu F, Peng Y Y, Wu J, Li Q, Zhang S Y and Qian Y T 2002 Microwave-templated synthesis of CdS nanotubes in aqueous solution at room temperature *New J. Chem.* **26** 1440–2
[50] Shao M W, Wu Z C, Gao F, Ye Y and Wei X W 2004 Surfactant-free route to hexagonal CdS nanotubes under ultrasonic irradiation in aqueous solution at room temperature *J. Cryst. Growth* **260** 63–6
[51] Zhou S M, Feng Y S and Zhang L D 2003 A two-step route to self-assembly of CdS nanotubes via electrodeposition and dissolution *Eur. J. Inorg. Chem.* **2003** 1794–7
[52] Shen X P, Yuan A H, Wang F, Hong J M and Xu Z 2005 Fabrication of well-aligned CdS nanotubes by CVD-template method *Solid State Commun.* **133** 19–22
[53] Thomas D G and Hopfield J J 1962 Optical properties of bound exciton complexes in cadmium sulfide *Phys. Rev.* **128** 2135
[54] Johnson P B and Christy R W 1972 Optical constants of the noble metals *Phys. Rev.* B **6** 4370–9
[55] Dong L F, Jiao J, Coulter M and Love L 2003 Catalytic growth of CdS nanobelts and nanowires on tungsten substrates *Chem. Phys. Lett.* **376** 653–8
[56] Pan A L, Liu D, Liu R B, Wang F F, Zhu X and Zou B S 2005 Optical waveguide through CdS nanoribbons *Small* **1** 980–3
[57] Zhai T, Fang X, Li L, Bando Y and Golberg D 2010 One-dimensional CdS nanostructures: synthesis, properties, and applications *Nanoscale* **2** 168–87
[58] Cao J, Sun J Z, Hong J, Li H Y, Chen H Z and Wang M 2004 Carbon nanotube/CdS core–shell nanowires prepared by a simple room-temperature chemical reduction method *Adv. Mater.* **16** 84
[59] Tak Y, Hong S J, Lee J S and Yong K 2009 Fabrication of ZnO/CdS core/shell nanowire arrays for efficient solar energy conversion *J. Mater. Chem.* **19** 5945–51
[60] Barrelet C J, Greytak A B and Lieber C M 2004 Nanowire photonic circuit elements *Nano Lett.* **4** 1981–5
[61] Ma R-M, Dai L, Huo H-B, Xu W-J and Oin G G 2007 High-performance logic circuits constructed on single CdS nanowires *Nano Lett.* **7** 3300–4
[62] Pyayt A L, Wiley B, Xia Y, Chen A and Dalton L 2008 Integration of photonic and silver nanowire plasmonic waveguides *Nature Nanotechnol.* **3** 660–5
[63] Yan R X, Pausauskie P, Huang J X and Yang P D 2009 Direct photonic–plasmonic coupling and routing in single nanowires *Proc. Natl Acad. Sci. USA* **106** 21045–50
[64] Wei H and Xu H X 2012 Nanowire-based plasmonic waveguides and devices for integrated nanophotonic circuits *Nanophotonics* in press